J Nanopart Res (2012) 14:883
DOI 10.1007/s11051-012-0883-8

RESEARCH PAPER

Species selection for the design of gold nanobioreactor by photosynthetic organisms

Si Amar Dahoumane · Chakib Djediat · Claude Yéprémian · Alain Couté · Fernand Fiévet · Thibaud Coradin · Roberta Brayner

Received: 19 September 2011 / Accepted: 19 April 2012

Abstract The design of cell-based bioreactors for inorganic particles formation requires both a better understanding of the underlying processes and the identification of most suitable organisms. With this purpose, the process of Au^{3+} incorporation, intracellular reduction, and Au^0 nanoparticle release in the culture medium was compared for four photosynthetic microorganisms, *Klebsormidium flaccidum* and *Cosmarium impressulum* green algae, *Euglena gracilis* euglenoid and *Anabaena flos-aquae* cyanobacteria. At low gold content, the two green algae show maintained photosynthetic activity and recovered particles (ca. 10 nm in size) are similar to internal colloids, indicating a full biological control over the whole process. In similar conditions, the euglenoid exhibits a rapid loss of biological activity, due to the absence of protective extracellular polysaccharide, but could grow again after an adaptation period. This results in a larger particle size dispersity but larger reduction yield. The cyanobacteria undergo rapid cell death, due to their prokaryotic nature, leading to high gold incorporation rate but poor control over released particle size. Similar observations can be made after addition of a larger gold salt concentration when all organisms rapidly die, suggesting that part of the process is not under biological control anymore but also involves extracellular chemical reactions. Overall, fruitful information on the whole biocrystallogenesis process is gained and most suitable species for further bioreactor design can be identified, i.e., green algae with external coating.

Keywords Gold · Algae · Cyanobacteria · Biosynthesis · Bioreactors · Nanobiotechnology

S. A. Dahoumane · F. Fiévet · R. Brayner (✉)
Interfaces, Traitements, Organisation et Dynamique des Systèmes (ITODYS), UMR 7086, CNRS, Sorbonne Paris Cité, Université Paris Diderot, 15 Rue Jean de Baïf, 75205 Paris Cedex 13, France
e-mail: roberta.brayner@univ-paris-diderot.fr

C. Djediat · C. Yéprémian · A. Couté
Département RDDM, FRE 3206, USM 505, Muséum National d'Histoire Naturelle, 57 Rue Cuvier, 75005 Paris, France

T. Coradin (✉)
CNRS, Chimie de la Matière Condensée de Paris (LCMCP), Collège de France, UPMC Universités Paris 06, 11 Place Marcellin Berthelot, 75005 Paris, France
e-mail: thibaud.coradin@upmc.fr

Introduction

The ability of living organisms to form nanoparticles, organic (lipid granules, Thomson et al. 2010), polyesters (Sudesh et al. 2000), and inorganic (metal, metal oxide) (Beveridge et al. 1997; Klaus-Joerger et al. 2001; Korbekandi et al. 2009; Narayanan and Sakthivel 2010), intracellularly is now well recognized. These biocontrolled routes provide a promising alternative to chemical syntheses, not only due to their environmental-friendly conditions (green

Published online: 03 June 2012

nanochemistry) but also because they rely on the whole cellular machinery (Mandal et al. 2006; Dahl et al. 2007). As a result, the cells can exert a precise control over monomer (or ion) uptake, provide confined compartments for polymerization (or nucleation/growth) and, in some case, permit the externalization of biocolloids (Mann 2008; Virkutyte and Varma 2011). On this basis, it can be expected that a careful selection of living organisms and/or a rational design of growth conditions can allow the optimization of the biosynthesis/recovery processes, paving the way to the development of cell-based nanobioreactors (Wu and Payne 2004).

Among inorganic nanoparticles, the biosynthesis of gold colloids has probably been the most studied (Das and Marsili 2010). This interest is very likely to be due to gold-specific optical properties at the nanoscale and to its wide range of applications (Eustis and El-Sayed 2006). In addition, due to the easy chemical reduction of Au(III) salts, a wide range of living organisms, such as bacteria, fungi, algae, and even human cells, has been observed to contain gold nanoparticles intracellularly (Ahmad et al. 2003; Anshup et al. 2005; Lengke et al. 2006; Brayner et al. 2007; however, the underlying processes are still unclear. On the one hand, recent studies on bacteria suggest extracellular reduction and uptake to the cytoplasmic space, suggesting a non-enzymatic process (De Corte et al. 2011). A similar process was suggested for some marine algae, but no intracellular nanoparticles were observed (Vijayaraghavan et al. 2011). On the other hand, in several algae, gold nanoparticles were mainly localized in the thylakoidal membranes (Brayner et al. 2007). In addition, chloroplasts contain reducing enzymes that were previously suggested to be involved in intracellular metal salt reduction (Kumar et al. 2007).

In this context, this study aims at getting a better understanding of the processes involved the intracellular biocrystallogenesis of gold nanoparticles to identify the most suitable organisms for the design of a cell-based nanobioreactor (Sicard et al. 2010; Dahoumane et al. 2012). With this aim, we selected different photosynthetic organisms with specific physiological features. We show here that a combination of structural, chemical, and biological analyses allows the monitoring of the whole process from Au^{3+} salt addition to Au^0 nanoparticle release. These data enlighten the role of intrinsic metal tolerance and extracellular biopolymer (extracellular polymeric substance, EPS) coating on the course of the biocrystallogenesis reaction, allowing the identification of eukaryotic EPS-coated green algae as the best candidates for further biotechnological developments.

Experimental section

Photosynthetic microorganism description and culture

Four photosynthetic organisms with distinct structural or physiological features were selected: *Cosmarium impressulum* (*Ci*), a planktonic single-celled eukaryotic green algae coated with an EPS; *Klebsormidium flaccidum* (*Kf*), a benthic filamentous eukaryotic green algae with EPS; *Euglena gracilis* (*EgM*), a single-celled eukaryotic euglenoid without EPS; *Anabaena flos-aquae* (*Af*), a planktonic filamentous prokaryotic cyanobacteria with EPS. *Ci*, *EgM*, and *Af* came from MNHN Culture Collection. *Kf* was isolated from a sample of a black soiling developing on building near Paris (France).

All the microorganisms, except *EgM*, were grown in 250-ml Erlenmeyer flasks, in sterile Bold's basal (BB) medium and buffered with 3.5 mM phosphate buffer at a controlled temperature of 20.0 ± 0.5 °C and luminosity (50–80 µmol m^{-2} s^{-1} Photosynthetic Photon Flux (PPF) for *Kf* 30–60 µmol m^{-2} s^{-1} PPF for *Ci* and *Af* under ambient CO_2 conditions. The pH of the medium was adjusted to 7 using 1 M NaOH solution. *EgM* was grown in 250-mL Erlenmeyer flasks, in Mineral (M) medium at a control temperature of 20.0 ± 0.5 °C and luminosity (70–100 µmol m^{-2} s^{-1} PPF) under ambient CO_2 conditions. The pH of the medium was adjusted to 3.6 using 1 M HCl solution.

Before addition of gold salts, the culture was transferred (10 % (v/v) of inoculum) into the culture medium, and grown for 2 weeks. Resulting samples are termed Organism 1 and Organism 2 for 10^{-3} M and 10^{-4} M $HAuCl_4$ concentrations, respectively.

Microalgae and nanoparticle characterization

Optical microscopy was performed with a Zeiss Primo Star microscope. The photosynthetic activity of the microalgae was measured using the pulsed amplitude

modulation (PAM) method with a Handy PEA (Hansatech instruments) fluorometer (Ritchie 2008). This method uses the saturation pulse method, in which a phytoplankton sample is subjected to a short beam of light that saturates the photosystem II (PSII) reaction centers of the active chlorophyll molecules. This process suppresses photochemical quenching, which might otherwise reduce the maximum fluorescence yield. A ratio of variable over maximal fluorescence (F_v/F_m) can then be calculated which approximates the potential quantum yield of PSII, with F_m, maximal fluorescence yield of a dark-adapted sample, with all PSII reaction centers fully closed F_0, minimal fluorescence yield of a dark-adapted sample, with all PSII reaction centers fully open and $F_v = F_m - F_0$, termed the variable fluorescence.

The chlorophyll *a* was extracted from 1 mL of unicellular algal culture in 9 mL of acetone. After 1 min of vortex, the solution was heated at 37 °C during 3 min followed by centrifugation. The evolution of chlorophyll *a* band, centered at 663 nm, was followed by UV–Vis spectroscopy, using a Cary 5E spectrophotometer.

Biomass transmission electron microscopy (TEM) imaging was performed with a Hitachi H-700 operating at 75 kV equipped with a Hamatsu camera. For TEM studies, the microalgae were fixed with a mixture containing 2.5 % of glutaraldehyde, 1.0 % of picric acid in a phosphate Sörengen Buffer (0.1 M, pH 7.4). Dehydration was then achieved in a series of ethanol baths, and the samples were processed for flat embedding in a Spurr resin. Ultrathin sections were made using a Reicherd E Young Ultracut ultramicrotome (Leica). Sections were contrasted with ethanolic uranyl acetate before visualization. Mean particle diameters were estimated from image analysis of more than 150 particles using a digital camera and the SAISAM and TAMIS software for statistical analyses (Microvision Instruments).

Scanning electron microscopy using field emission gun (SEM–FEG) was performed using Zeiss Supra 40 operating at 20 kV. Secondary Electron Detector was used. Prior to observation, the samples were fixed with glutaraldehyde, dehydrated in acetone, and dried with a critical point dryer BAL-TEC CPD 030 with liquid CO_2; critical point 31 °C–73.8 bar.

X-ray photoelectron spectroscopy (XPS) was performed in a Thermo VG Scientific Sigma Probe spectrometer equipped with a monochromatic AlKα X-ray source (1486.6 eV) used at a spot size of 400 μm. The pass energy was set at 100 and 40 eV for the survey and the high-resolution spectra, respectively. The step size was 1 eV for the survey spectrum and 0.2 eV for the high-resolution spectra. Charge compensation was achieved with a flood gun of 6 eV using standard procedures for this spectrometer. The surface composition was determined using the manufacturer's sensitivity factors. The analyses were performed on whole cells after centrifugation, washing, and freeze-drying. The gold weight content was obtained by chemical analyses at the CNRS analytic platform (Vernaison, France).

Powder X-ray diffraction (XRD) experiments were carried out on an X'Pert Pro Panalytical diffractometer equipped with a Co anode ($\lambda = 0.17889$ nm) and a multichannel detector (X'Celerator) in the 40–80 2θ range (0.054 step). The patterns were indexed and the size of the coherent diffraction domains (crystallites) inferred from line broadening analysis was determined with HIGHSCORE software (Panalytical) using the Scherrer's formula, the experimental broadening being corrected from the instrumental broadening from analysis of well-crystallized Si samples. For the diffraction, only 30 mg of freeze-dried samples was needed.

Results

In these experiments, $HAuCl_4$ aqueous solutions were added to the culture media containing the microorganisms. Cultures were placed into the incubator (20 °C, 16 h light/8 h dark) until observation of color modification of the biomass and/or the culture medium to purple, suggesting gold metallic nanoparticles formation (Fig. 1).

In a first step, the evolution of culture media content with time was followed by UV–Vis spectroscopy (Fig. 2). At 10^{-3} M gold concentration, nanoparticles could only be detected in the culture medium of *Kf*, whereas significant absorption bands in the visible range could be observed for all organisms at 10^{-4} M. For *Kf 1*, the UV–Vis spectra presents a narrow surface plasmon resonance (SPR) band at $\lambda_{max} \sim 540$ nm after 1 day that grows in intensity over 1 week while experiencing a significant ($\sim$20 nm) red shift (Fig. 2a). For *Kf 2*, a similar SPR band becomes detectable after 3 days and rises in intensity over

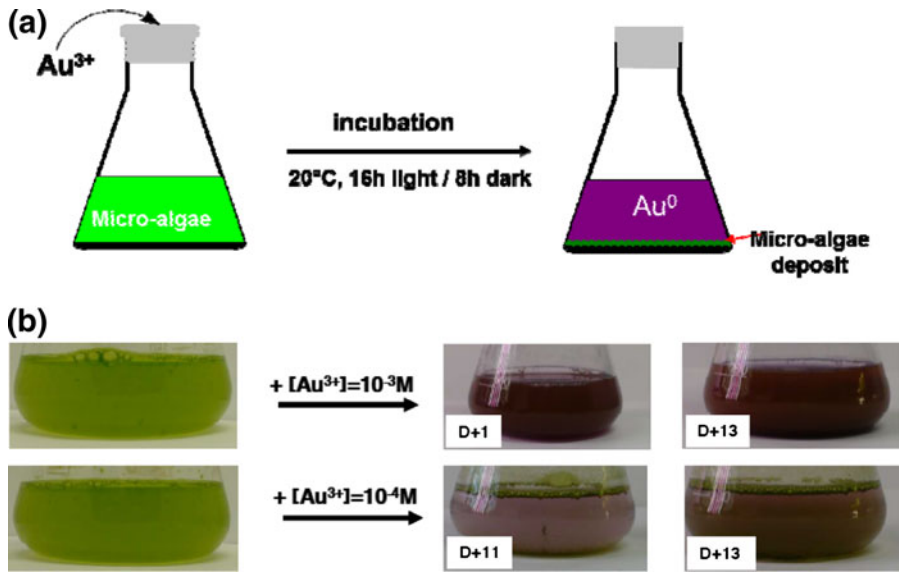

Fig. 1 **a** Scheme of the biosynthesis of gold nanoparticles and **b** color changes of biomass and culture medium after reduction reaction. (Color figure online)

9 days but the final maximum absorption is about ten times lower than for *Kf 1* (Fig. 2b). For *EgM 2*, an asymmetric SPR band at $\lambda_{max} \sim 510$ nm was observed after 1 day, whose intensity decreases with time (Fig. 2c). *Ci 2* follows a similar trend except that only a broad band was observed in the 500–700-nm region (Fig. 2d) Culture medium of *Af 2* shows a similar evolution as *Kf 2* except that the absorption intensity increases up to 13 days (Fig. 2e). Selected TEM micrographs of gold nanoparticles recovered from the culture medium are shown in Fig. 3. All the nanoparticles are spherical and surrounded by an organic matrix of variable density. Noticeably, particles could be visualized for all samples and at both gold salt concentration, indicating that UV–Vis spectroscopy is not sensitive enough to detect low amount of gold particles in the culture medium. Table 1 presents the mean diameter (ϕ_r) of the nanoparticles that sometimes exhibit large size distribution. Interestingly, the average particle size appears smaller for the highest gold concentration for *Ci*, *Kf*, and *Af* and is constant for *EgM 1* and *EgM 2*. It is important to point out that in the absence of cells, no gold reduction was observed, even when extracted EPS was present.

In a second step, analyses were focused on the intracellular gold content that could be ascertained by the cell color change of all the microorganisms from green to pink or purple after suitable incubation time (Fig. 4). Figure 5 shows TEM micrographs of microorganism thin sections after production of gold nanoparticles that are found inside the vegetative cells. They appear most specifically located on the thylakoids for *Ci* and *Kf* but more dispersed for *EgM* and *Af*. The corresponding estimated mean diameters (ϕ_i) are reported in Table 1. When compared to colloids found in the culture medium, it is worth noting that size dispersion is much smaller with a negligible range of gold concentration dependence ($\Delta\phi_i \sim 2$ nm for both the parameters, i.e., below particle size dispersity).

Further analyses were performed on freeze-dried cells. As shown on Fig. 6, SEM–FEG micrographs indicate that, in the case of *Ci 1* and *Af 1* (not shown), the particles on the microorganism surface are in the micron range and they present most triangular shape. For *EgM 1*, a mixture of triangular and spherical shape particles ca. 100 nm in size is observed. In all other conditions, the nanoparticles present a spherical shape with diameter 50 nm or below. They are well dispersed on the surface, except for *Ci 2* where they appear as aggregates on very specific sites of the outer cell wall. In parallel, XRD patterns of freeze-dried cells (Fig. 7) allow the calculation of the mean crystallite sizes (L) (Table 1). These data confirm the trends of SEM–FEG observation, i.e., a decrease in particle size with decreasing gold concentration.

Chemical analyses and XPS studies were performed on centrifuged and washed freeze-dried cells after 15 days of contact with metal salts to characterize further the gold reduction process. As indicated in

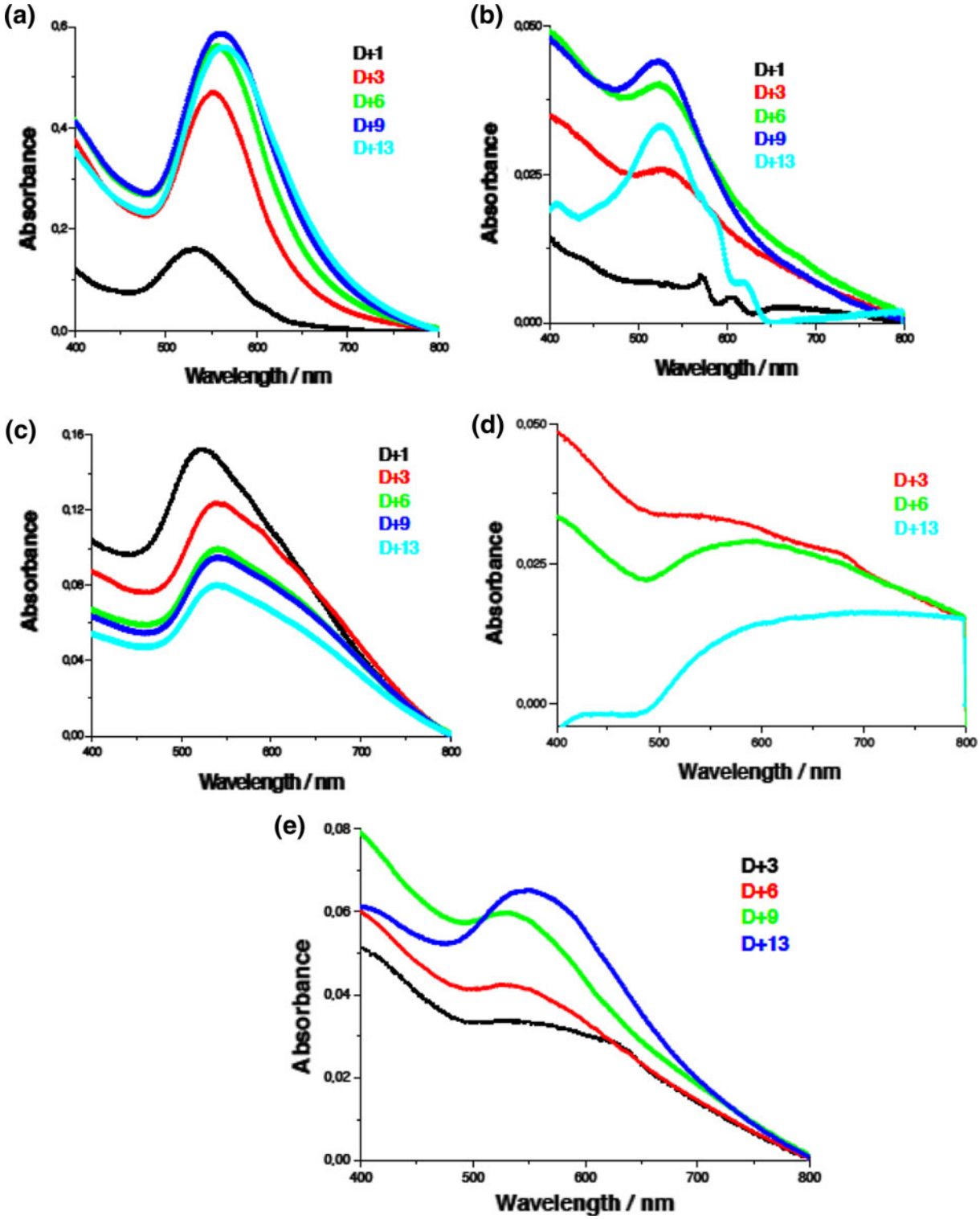

Fig. 2 Evolution of UV–Vis spectra as a function of the time after gold salt addition for the culture media containing **a** *Kf 1*, **b** *Kf 2*, **c** *Ci 2*, **d** *EgM 2*, and **e** *Af 2*

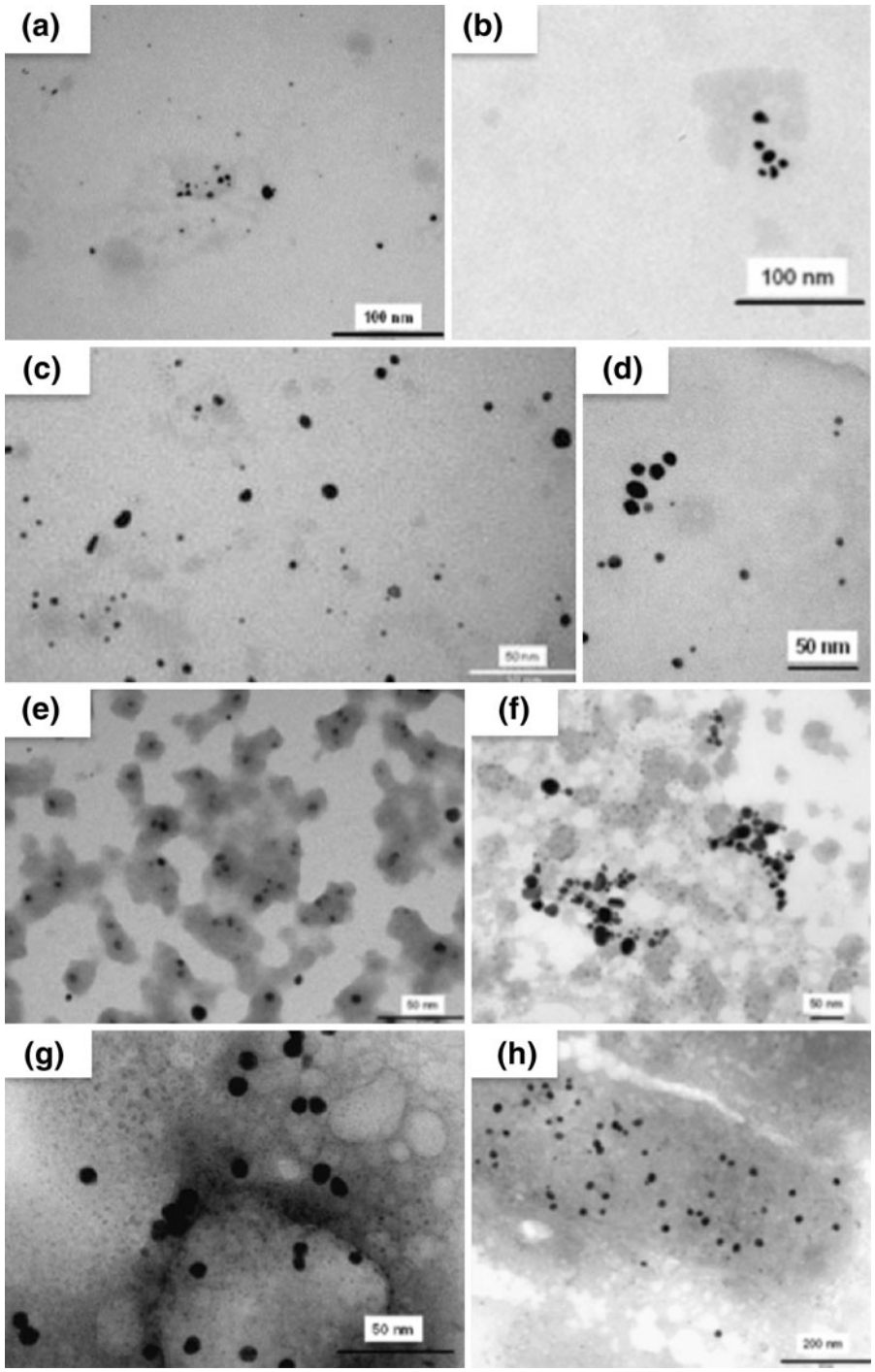

Fig. 3 TEM micrographs of released gold nanoparticles in the culture media of **a** *Ci 1*, **b** *Ci 2*, **c** *Kf 1*, **d** *Kf 2*, **e** *EgM 1*, **f** *EgM 2*, **g** *Af 1*, and **h** *Af 2*

Table 1, *Ci* showed the lowest gold content (15–20 wt%) among the four species under study. In contrast, *Kf* was associated with the highest gold concentration for *Kf 1* (ca. 80 wt%) but a very low concentration for *Kf 2* (ca. 15 wt%). *EgM* and *Af* show intermediate gold content (40 and 60 wt%,

Table 1 Interspecies variations in total gold content (Au, wt%), reduction yield (Au^0/Au), internal (ϕ_i) and released (ϕ_r) particle mean diameter and mean crystallite size (L) as a function of initial gold salt concentration

Sample	$[Au^{3+}]$ (M)	Au (wt%)[a]	Au^0/Au_{total}[b]	ϕ_i (nm)[c]	ϕ_r (nm)[c]	L (nm)[d]
Ci 1	10^{-3}	20	0.78	10.3 ± 7.2	4.5 ± 1.5	54
Ci 2	10^{-4}	14	0.77	12.3 ± 1.3	8.0 ± 3.0	11
Kf 1	10^{-3}	78	0.95	7.9 ± 1.4	5.0 ± 1.7	36
Kf 2	10^{-4}	16	0.81	9.0 ± 3.4	8.6 ± 4.2	7
EgM 1	10^{-3}	42	0.68	9.3 ± 2.8	11.1 ± 4.2	72
EgM 2	10^{-4}	41	0.86	11.3 ± 9.7	11.3 ± 4.7	12
Af 1	10^{-3}	61	0.64	10.0 ± 4.7	7.9 ± 1.5	91
Af 2	10^{-4}	59	0.82	8.1 ± 2.1	14.8 ± 5.3	23

[a] ±1 from chemical analyses

[b] ±0.01, from XPS

[c] From TEM

[d] From XRD

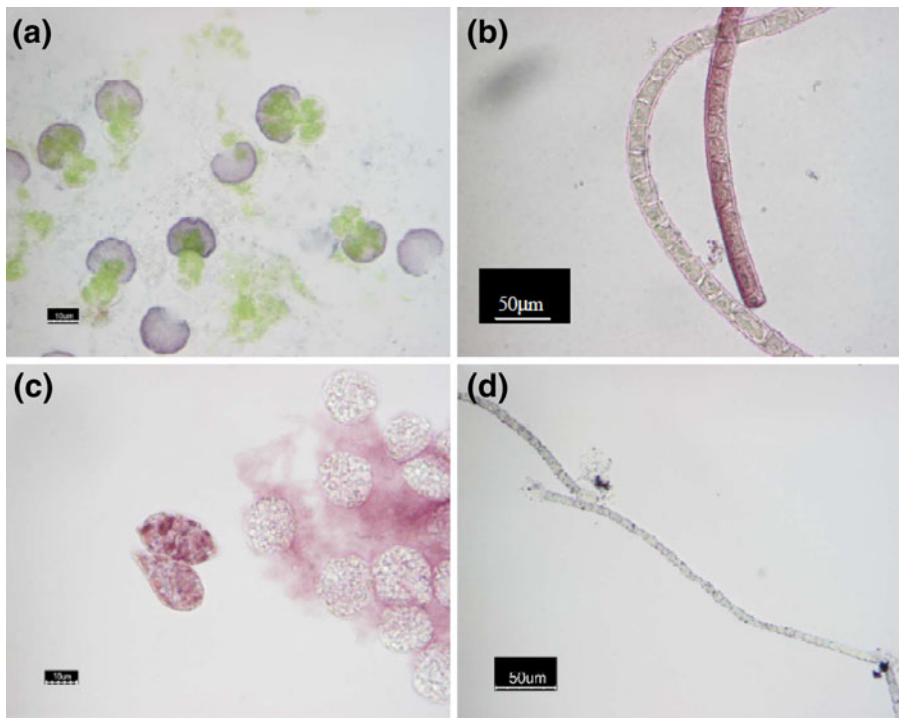

Fig. 4 Photonic micrographs of **a** *Ci 1*, **b** *Kf 1*, **c** *EgM 1*, and **d** *Af 1*. (Color figure online)

respectively), independently of initial salt concentration. In parallel, XPS spectra revealed that Au^{3+} and Au^0 species coexist on and/or within the cells (Fig. 8). Au4f region was fitted with four components centered at 84.0 and 87.9 eV assigned to metallic Au and 85.5 and 89.3 eV assigned to Au^{3+} species (84.0 and 85.5 eV for $Au4f_{7/2}$ and 87.9 and 89.3 eV for $Au4f_{5/2}$). The calculated Au^0/Au_{total} ratio, shown in Table 1, indicates a range of 0.65 (for *Af 1*) to 0.95 (for *Kf 1*) but no specific trend in terms of interspecies variation and/or influence of initial gold content could be identified.

We then focused our attention on the impact of gold reduction on the physiological state of the cells. Before addition of gold salts, the photosynthetic activity (F_v/F_m), as monitored using PAM spectroscopy, of all the microorganisms remains stable during

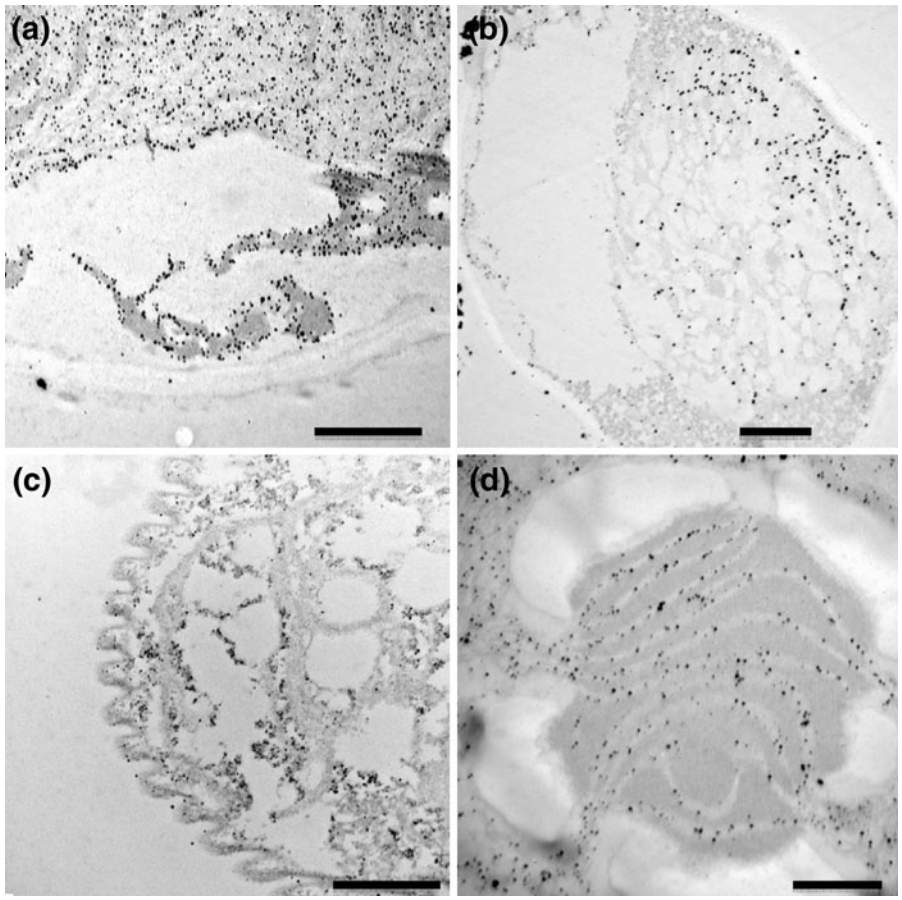

Fig. 5 TEM micrographs of microorganism thin sections for **a** *Ci 2*, **b** *Kf 2*, **c** *EgM 2*, and **d** *Af 2* (*scale bar* 500 nm)

more than 2 months and the F_0, F_m, and F_v parameters increase with time (data not shown). After addition of $[Au^{3+}] = 10^{-3}$ M, for all the microorganisms, the decrease of the photosynthetic activity was followed by cell death, as illustrated for *Kf 1* in Fig. 9a. After addition of $[Au^{3+}] = 10^{-4}$ M, *Kf 2* and *Ci 2* showed maintained photosynthetic activity while *EgM 2* underwent a rapid loss of activity followed, after an adaptation period, of a novel growth period (Fig. 9b, c). In the case of *Af 2* (Fig. 9d), gold addition led to rapid cell death. Parallel analyses were performed following the UV–Vis absorption spectra of chlorophyll *a*. Unfortunately, this method can be used only for unicellular species so that filamentous *Kf* and *Af* were not analyzed. As shown in Fig. 10, the chlorophyll *a* band disappears 1 week after gold addition for the high salt concentration (*Ci 1* and *EgM 1*, Fig. 10a, c) but increases in intensity over 2 weeks for *Ci 2* (Fig. 10b) while showing a decrease followed by an increase for *EgM 2* (Fig. 10d), in good agreement with PAM data.

Finally, to contribute the understanding of the intracellular process involved in gold reduction, we attempt to identify putative reducing enzymes that would be specifically located in the thylakoidal membranes. Based on the literature (He et al. 2007), we selected a NAD(P)H-dependent enzyme, nitrate reductase that was mixed with its coenzyme NAD(P)H within polysaccharides (PS) extracted from *Ci*. The presence of PS is used as model of both spatial confinement as occurring within thylakoids and as the environment of particles when they escape the cells. Interestingly, the reduction was observed only when both the enzymes were present (Fig. 11). UV–Vis spectra show an SPR band centred at 510 nm. The resulting nanoparticles are well dispersed in the medium and are larger (20 nm) than those produced in vivo by *Ci*.

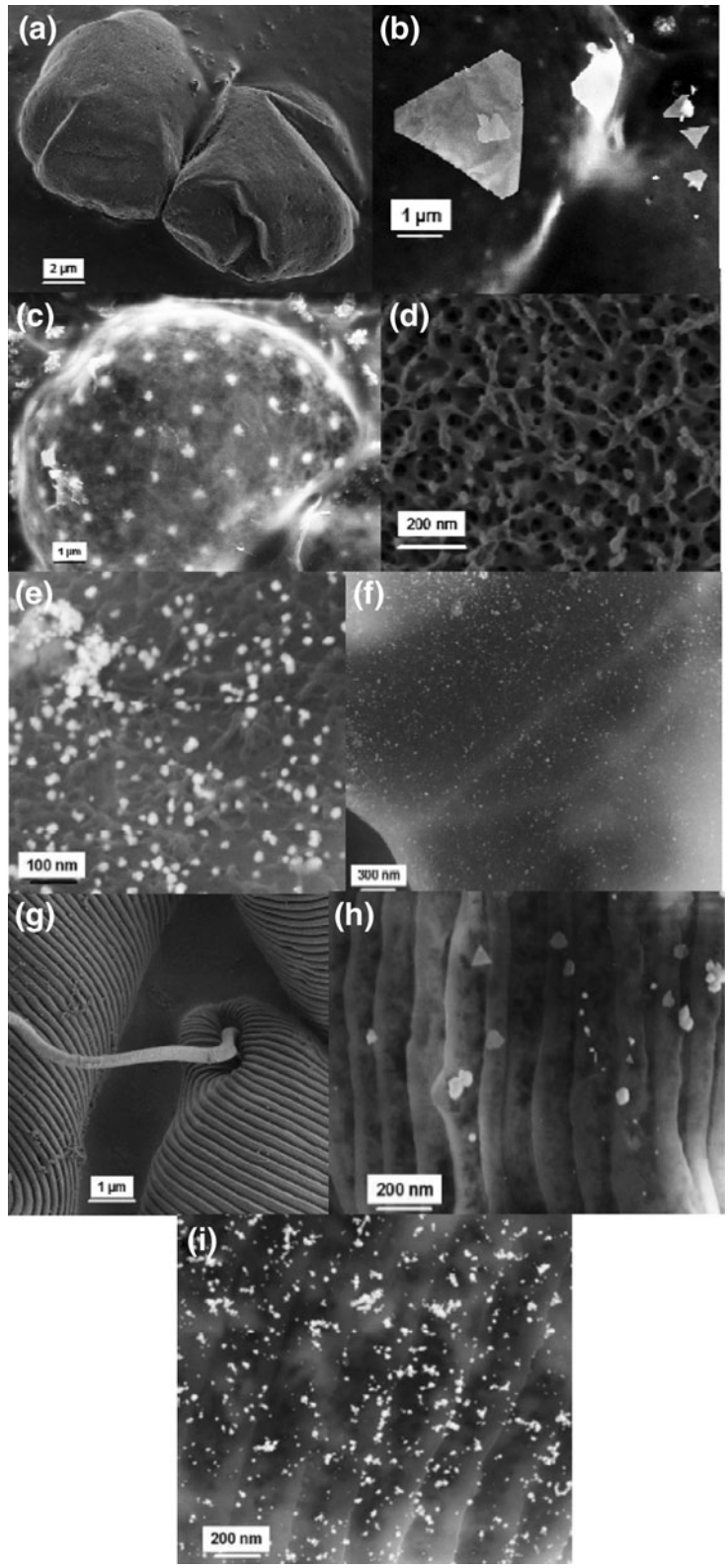

Fig. 6 SEM–FEG micrographs of the surface of **a** *Ci*, **b** *Ci 1*, **c** *Ci 2*, **d** *Kf*, **e** *Kf 1*, **f** *Kf 2*, **g** *EgM*, **h** *EgM 1*, and **i** *EgM 2*

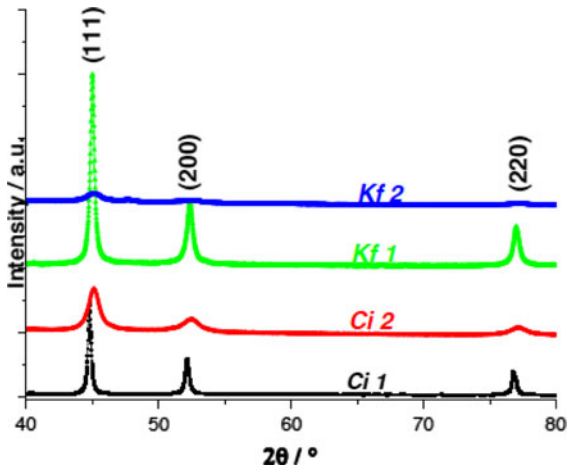

Fig. 7 Selected XRD patterns of lyophilized algae after 15 days of contact with gold salts

Fig. 9 Evolution of the photosynthetic activities of the microorganisms with time (in days) for **a** *Kf 1*, **b** *Kf 2*, **c** *EgM 2*, and **d** *Af 2* as monitored by the PAM technique. F_0, F_m, and F_v are the minimal fluorescence yield, the maximal fluorescence yield, and the variable fluorescence for a dark-adapted sample, respectively, and F_v/F_m is the photosynthetic efficiency of the PSII system

Discussion

Cell viability

Considering the different species, three situations arise. *Ci* and *Kf* are eukaryotic green algae coated with EPS. They are, therefore, expected to be less impacted by gold addition, both from slowing down of metal salt diffusion thanks to the polymer coating and to intrinsic

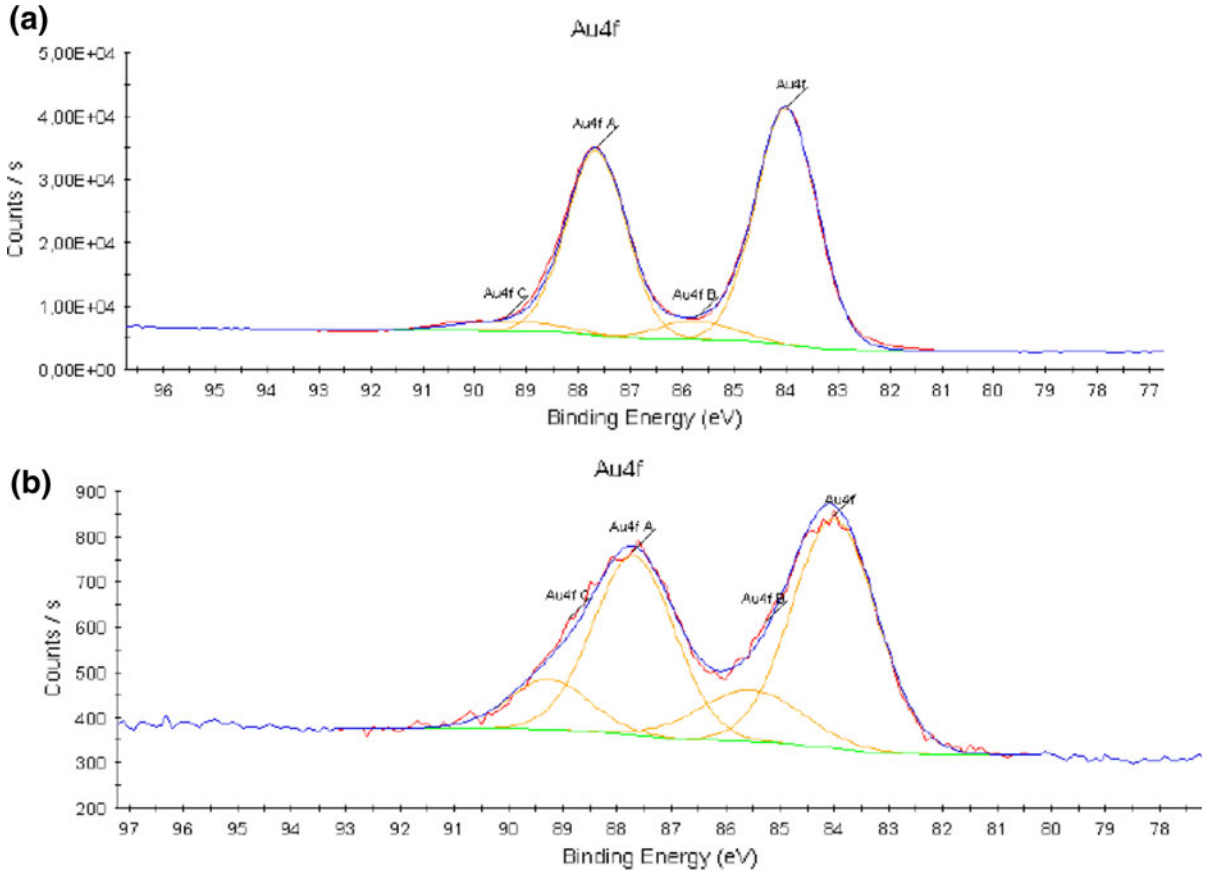

Fig. 8 XPS core-level Au4f region. **a** *Kf 1* and **b** *Kf 2*

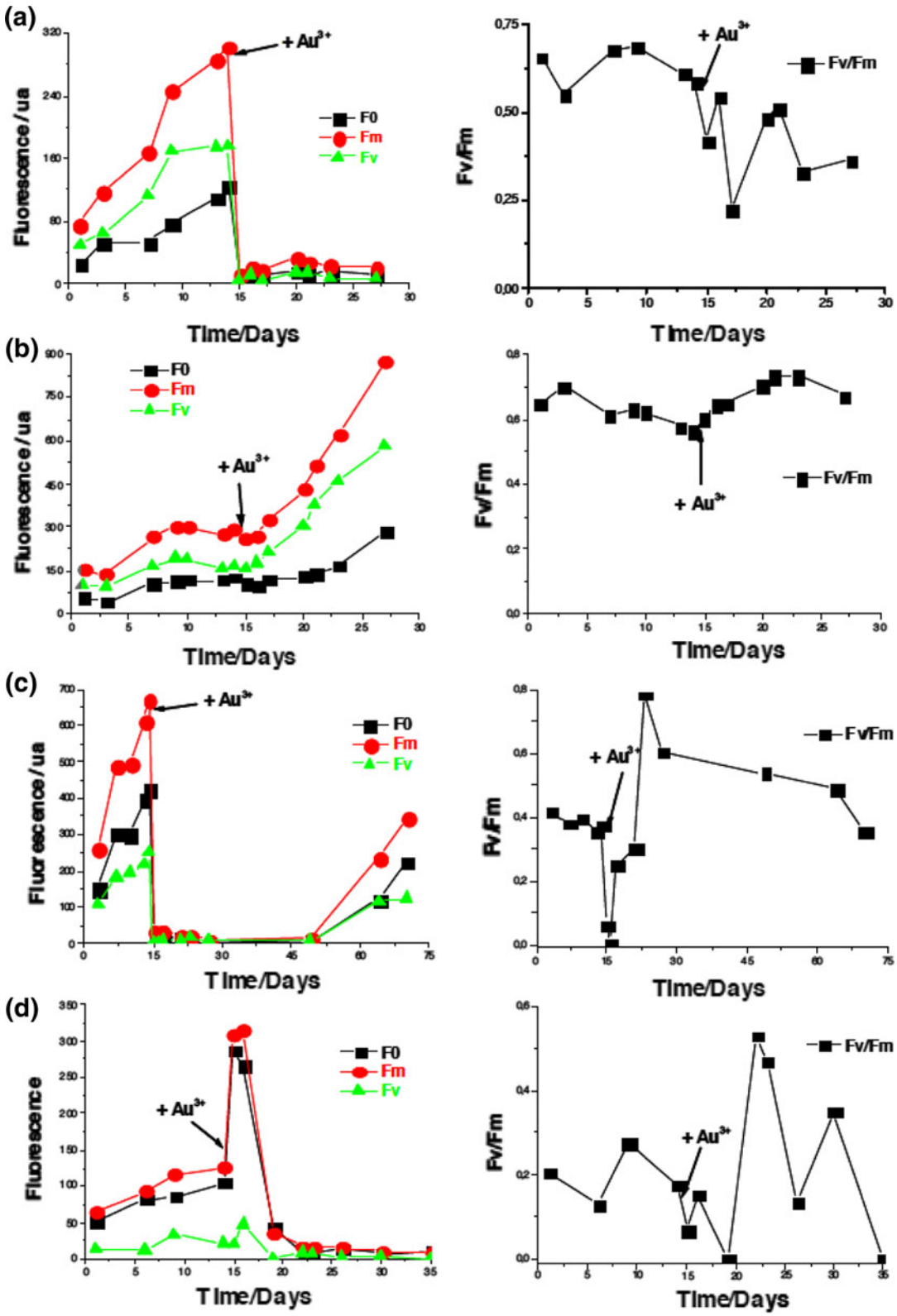
(a)
Fluorescence/ua
Time/Days
F0
Fm
Fv
+ Au3+
Fv/Fm
(b)
Fluorescence/ua
Time/Days
F0
Fm
Fv
+ Au3+
Fv/Fm
(c)
Fluorescence/ua
Time/Days
F0
Fm
Fv
+ Au3+
Fv/Fm
(d)
Fluorescence
Time/Days
F0
Fm
Fv
+ Au3+
Fv/Fm

high metal resistance due to their eukaryotic nature (i.e., compared to prokaryotic cells) (Reddy et al. 2007). *EgM* is also eukaryotic green algae but deprived of EPS so gold diffusion into the cell should be faster, resulting in a more significant sensitivity to gold content. A higher sensitivity is also expected for *Af* despite the presence of EPS, as a consequence of its prokaryotic nature. All these expectations are verified by PAM and chlorophyll *a* monitoring at the lowest gold salt content (10^{-4} M). The growth of *Ci* and *Kf* is not significantly perturbed upon metal salt addition, whereas *EgM* undergoes a rapid loss of photosynthetic activity followed by an adaptation period after which cells start to grow again and *Af* rapidly dies without recovery. Noticeably, all the cells undergo rapid death after 10^{-3} M $HAuCl_4$ addition, suggesting that neither the intrinsic resistance of eukaryotic cells nor the EPS coating can efficiently decrease the toxical effect of the metal ions (Scheme 1).

Gold nanoparticle characterization

Gold nanoparticles could be observed within the cells, on the cell outer surface and in the culture medium. Different situations should be envisioned: (i) gold reduction can occur in solution, inside the EPS or within the cells; (ii) particles can enter/escape the cells by endocytosis/exocytosis or through damaged cell wall. In the case of *Ci* at low initial gold concentration, particles found inside or outside the cells have similar size inferred from TEM (ca. 10 nm), close to the value of the crystallite size inferred from XRD line broadening. Therefore, these nanoparticles can be considered as single crystals even if there is probably a

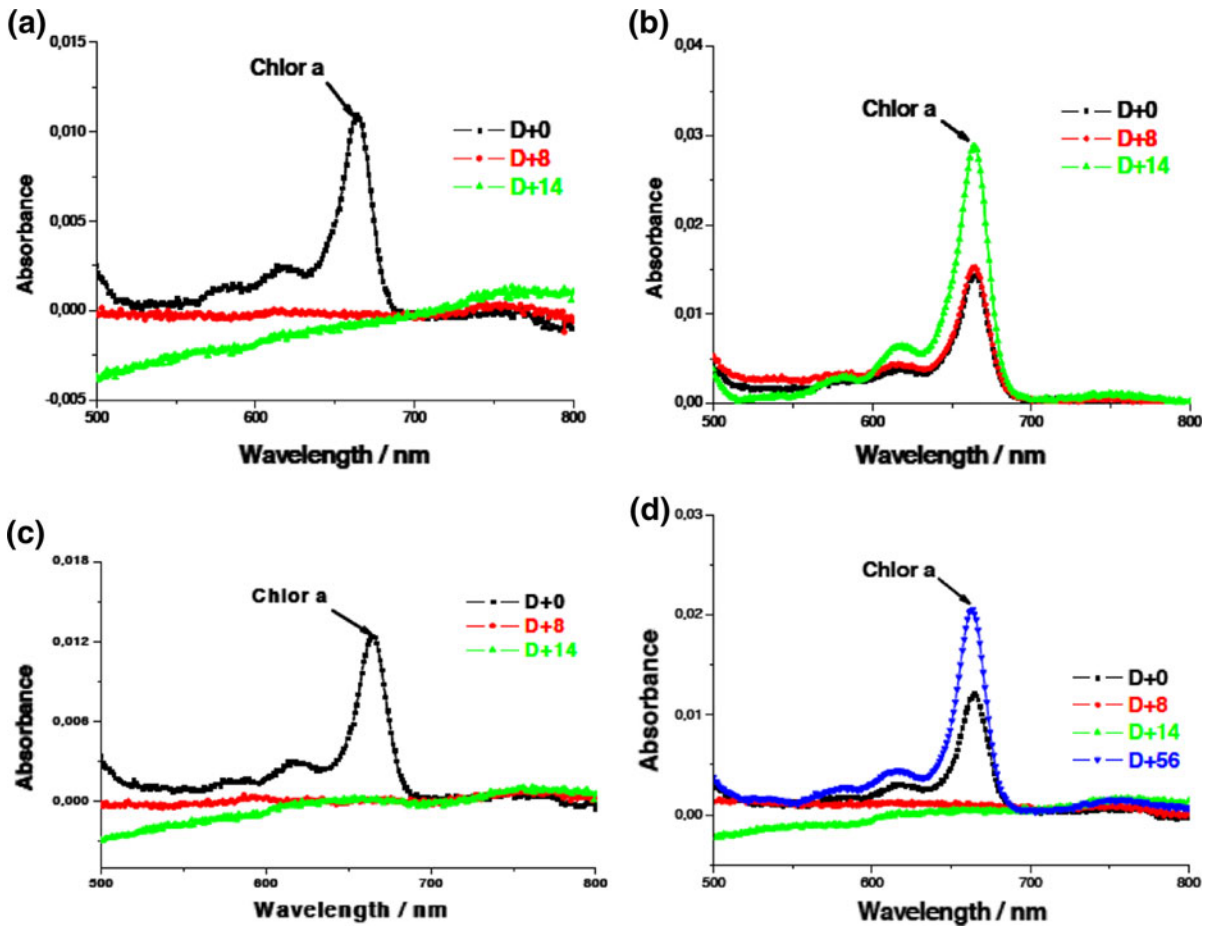

Fig. 10 UV–Vis monitoring of chlorophyll *a* absorption for **a** *Ci 1*, **b** *Ci 2*, **c** *EgM 1*, and **d** *EgM 2*

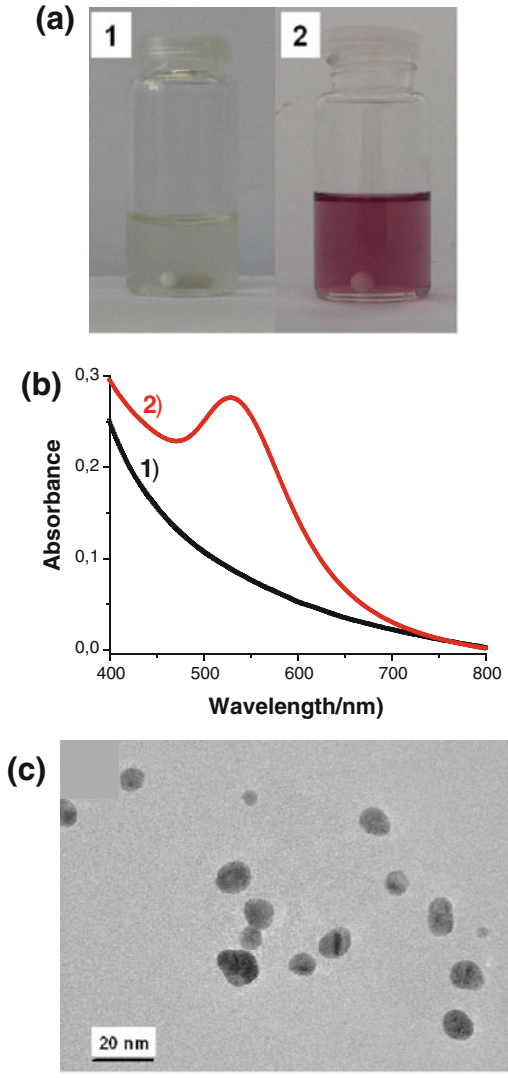

Fig. 11 **a** In vitro synthesis of gold nanoparticles in the presence of *Ci* extracted PS, $[Au^{3+}] = 10^{-4}$ M and (*1*) NAD(P)H (5×10^{-4} M), (*2*) commercial nitrate reductase + coenzyme NAD(P)H (1.5 mg/mL), **b** corresponding UV–Vis spectra, and **c** TEM image of sample 2

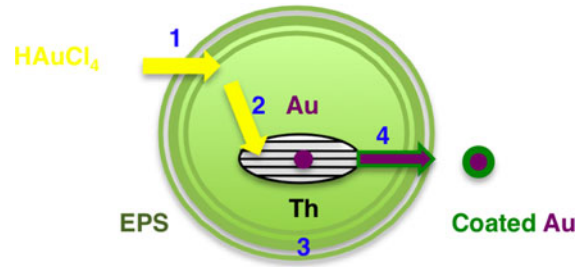

Scheme 1 Schematic overview of the process. (*1*) $HAuCl_4$ gold salts enter the cell through the EPS coating, (*2*) diffuse intracellularly to the thylakoidal membranes (Th), (*3*) where they are reduced in metallic gold (Au), and (*4*) are released surrounded by a polymeric coating

certain disorder near their surface. Because in these conditions cells survive the gold addition process, the transport of particle through damaged membrane can be discarded. This assumption is supported by SEM–FEG images suggesting that part of the particles remains trapped within the EPS, defining a remarkably regular pattern of aggregates that may correspond to specific pores (Lang and Fay 1971). The question remains whether these particles are formed in the EPS and are uptake by the cells or if their intracellular localization is due to internal reduction. Another point to be clarified is related to the possibility for intracellular reduction within intermediate endosomal vesicles that contain reducing biomolecules. Although, a definite answer is difficult to provide at this time, it is worth noting that it has already been identified that thylakoidal storage of metal ions is a common detoxification strategy in photosynthetic organisms (Wong et al. 1994). In addition, TEM images indicate that metal nanoparticles are found very systematically in the chloroplasts and not in other organelles. Finally, reducing enzymes that are present in the chloroplasts have been suggested to be involved in the reduction process (Brayner et al. 2007; He et al. 2007; Kumar et al. 2007: Virkutyte and Varma 2011). For instance, hydrogenase enzyme (that is involved in the photosynthesis process) generates NAD(P)H coenzyme (cofactor) in the photosystem I (PSI) (Ghirardi et al. 2007). This coenzyme is a strong reductant that can act as reducing agent in the gold metallic nanoparticle reaction. This reaction may cause a drastic decrease of PSII activity and consequently a decrease of O_2 production, as observed here during the photosynthetic activity tests and chlorophyll *a* assays. The reduction seems to be initiated by electron transfer from NAD(P)H by NAD(P)H-dependent reductase as electron carrier. Then the gold ions gain electrons and are reduced to gold metallic nanoparticles. Our experiments, although they were performed on nitrate reductase instead of hydrogenase (that is not easily available), confirm that NAD(P)H-dependent enzymes are able to reduce gold ions. Noticeably, nanoparticles are well dispersed but exhibit larger size than colloids formed within the cells, indicating the PS coating can stabilize the particles but cannot strictly mimic the

dimension and flexibility of thylakoidal membranes. Therefore, it can be suggested that colloids associated with *Ci* are originating from the reduction of gold ions incorporated in the chloroplast and are released via cell wall pores into the EPS and then in the culture medium.

A rather similar process can be assumed for *Kf* at a similar 10^{-4} M concentration for which particle size is also similar for internal and recovered particles and in good agreement with crystallite size obtained from XRD. However, from SEM–FEG, these particles appear more dispersed within the EPS, in agreement with previous demonstration that particle diffusion outside the cells occurs through intercytoplasmic canals (Brayner et al. 2007). *EgM* appears as a different situation since external and internal particles share a similar size, but with significantly higher size dispersity for internal particles compared to *Ci* and *Kf*. This may result from fast accumulation of Au^{3+} in the thylakoids due to both the absence of EPS-mediated slow diffusion and some perturbation of membrane integrity due to the observed rapid but transient loss of photosynthetic activity.

Af cells represent a very different situation because all the observed phenomena related to gold colloids occur when cells are damaged so that the biological control over the process is limited. In particular, diffusion of Au^{3+} and formed nanoparticles can be assumed to be easier and faster, due to the loss of membrane integrity. It is interesting to note that gold nanoparticle intracellular localization, as observed by TEM, is less specific than for *Ci* and *Kf*. In this situation, we also observed that internal and external particle size is different, with larger particles outside the cells, as indicated by SEM, TEM, and XRD. Interestingly, these results are similar to the ones we obtained at a higher gold content (10^{-3} M) for all species, i.e., size difference between external and internal particles and polycrystalline structures. As all these situations correspond to rapid cell death, it is reasonable to assume that the processes are not under biological control anymore but involve extracellular and intracellular reduction combine with easy in/out transport through damaged membranes. Noticeably, for *Kf* and *Ci*, the size of internal particles is found above the size of released colloids, which may indicate that the latter are not originating from the cell interior but may have been formed in the EPS network. This is supported by the fact that these two species show an increase in Au^0/Au_{total} with increasing concentration, suggesting that additional reduction has occurred. The fact that *Af* also exhibits larger particle size on its surface when gold content is increased strengthens the hypothesis that such a colloidal growth is involving external gold species and is not under biological control. Finally, it is interesting to emphasize that *EgM* behaves similarly to *Af* with increasing gold content, allowing the suggestion that an EPS-coated cyanobacteria shows a similar sensitivity to metal salts than an EPS-free eukaryotic microalgae.

Taken together, these data allow a more extensive discussion of the gold nanoparticle formation process. The Au(III) species are first in contact with the EPS network, if present. Here, reduction can occur by a photochemical effect together with a possible chemical interaction with the PS, as already demonstrated for alginic acid (Jaouen et al. 2010). Reduction can also occur directly on the cell surface, as demonstrated for cyanobacteria (Lengke and Southam 2006). In this case, it was suggested that an intermediate Au(I) species would be involved, which can be stabilized by some cellular products. These two mechanisms are in good agreement with our data showing gold particle formation even with dead cells. However, some particles are also observed within the cells. In the case of dead cells, one may suggest that they correspond to pre-formed Au(0) particles penetrating damaged membranes. However, for living cells, the specific localization of these particles in the thylakoids strongly suggests that the gold precursor, being either in the form of Au(III) or stabilized Au(I) reach these specific compartments. This hypothesis is strengthened by the fact that metal transport within marine organisms is well known to occur via specific ligands (Hudson and Morel 1993). The process occurring within the thylakoids is more difficult to explain in details. Our experiments using nitrate reductase demonstrate that such reducing enzymes have the ability to convert Au(III) species into Au(0) particles so that parent hydrogenases located in the thylakoids can be responsible for the reduction process. However, photochemical processes may also contribute to this reduction reaction, as the strong interaction between photosynthesis and gold colloids has been reported recently (Biesso et al. 2008).

Investigation of the culture medium

TEM observations of the culture medium indicate the presence of gold nanoparticles surrounded by an organic material with variable density. Two interesting observations can be made: this material is found even for organisms that are originally deprived of EPS (i.e., *EgM* and *Af*) and its amount/density increases with gold content. It can, therefore, be proposed that this material corresponds to polymers excreted by the cells as an effect of the toxic stress induced by the metal salt (Sheng et al. 2005).

Indeed, such a coating should have an impact on the fate of particles in the culture medium. The monitoring of the SPR band by UV–Vis spectroscopy indicates that three phenomena are occurring: particle release (leading to increased SPR band intensity), aggregation (leading to SPR band spectra shift), and precipitation (leading to decreased SPR band intensity). At low gold concentration, in the presence of *Ci*, fast release is followed by aggregation and precipitation whereas *Kf* shows slow release before aggregation/precipitation, which may correspond to our previous suggestion of a different release route between single cell and filamentous species. At a similar initial gold content, *EgM* leads to a similar behavior as *Ci* except for a higher initial particle amount and more limited aggregation, underlining the effect of the initial EPS content For *Af* at 10^{-4} M, a similar trend to *Kf* at 10^{-3} M, i.e., progressive increase and limited aggregation, is observed that may be correlated with the rapid loss of viability observed for both systems.

Towards algae-based bioreactor design

Targeting the development of bioreactors that would use microalgae to produce gold nanoparticles, an important parameter to investigate is the rate of the reduction reaction. Because the UV–Vis spectra only gives access to the monitoring of suspended particles, the intensity of the SPR band does not reflect the overall yield of particle release. This yield can be established by examining the chemical analyses performed on freeze-dried cells after centrifugation and washing that indicate the relative weight content of gold (Au %) present both inside and at the surface of the cells, i.e., those particles that were not released. Based on these data, it can be observed that at low initial gold concentration, the larger release amount (i.e., smaller Au % associated with the cells) for *Ci* and *Kf* also correspond to the lowest SPR band intensity in the culture medium, whereas *EgM* and *Af* show lower release amount (i.e., higher Au %) but also higher SPR intensity. This can be associated to the fact that the aggregation/precipitation processes are favored for higher particle concentration. Increasing the initial gold concentration to 10^{-3} M, only slight variations in Au % are observed for *Ci*, *EgM*, and *Af* whereas no significant SPR bands could be obtained in the culture medium whereas *Kf* shows high Au % and SPR band intensity. As mentioned earlier, this situation is more difficult to discuss because all the organisms quickly die and the process is not under biological control anymore after a few hours. On this basis, the full yield of reduction (i.e., including released and cell-associated particles) is not only difficult to determine but may also not be the more relevant parameter to consider the efficiency of the bioreactor. It is more important to identify the balance between high initial gold concentration that produces large amounts of particles but impact strongly on cell viability, hindering the development of continuous reactors, and low initial content that leads to lower colloid concentrations but preserve cellular activity on the long term (Dahoumane et al. 2012). In this situation, the initial delay to observe significant particle production (ca. 1 day) becomes negligible compared to sustained release over weeks period.

Taken all together, these data indicate that EPS-coated green algae, such as *Ci* and *Kf*, should be preferred to EPS-deprived green algae (*EgM*) and cyanobacteria (*Af*) for the development of bioreactors due to better resistance to metal toxicity (up to 10^{-4} M $HAuCl_4$) and fast release kinetics. Resulting particles are single crystalline with low dispersity due to their biogenic origin (i.e., with no significant modification in particle size between intracellular compartments and the culture medium), an important feature for their possible applications. Finally, another advantage of these species is that the particles are released associated with a polymeric coating leading to precipitation but limited aggregation, which may not only favor their recovery but also have a positive impact on their toxicity (Moulton et al. 2010).

Conclusions

The ability of several living organisms to perform the intracellular synthesis of inorganic nanomaterials is not only a fascinating area but also a potential source of applications, especially for the design of cell-based bioreactors (Hennebel et al. 2009; Vijayakumar and Prasad 2009; Das et al. 2009). However, in both the cases, it is important to identify the best-suited organism in terms of metal tolerance and reduction yield as well as particle size and morphology (Grzelczak et al. 2008). This study highlights the different behaviors of prokaryotic versus eukaryotic cells, EPS-coated versus EPS-free algae and, to a smaller extent, single cell versus filamentous organisms. In addition, it demonstrates that a combination of biologically controlled and chemically controlled phenomena may occur depending on the cell physiology. Two main future fields of investigation can be foreseen: from a more fundamental point of view, it would be of high interest to perform in vitro experiments within isolated chloroplasts or artificial membranes, involving hydrogenase enzymes or mimicking systems. From a more applied perspective, the immobilization of the microalgae within solid supports would represent an important step towards the design of "living" bionanoreactors.

Acknowledgments The authors thank D. Montero and F. Herbst (ITODYS) for assistance in SEM–FEG experiments as well as J. Livage, and C. Sicard (LCMCP) for fruitful discussions. R.B. and T.C. thank the Ile-de-France region for funding support in the frame of the CNano IdF program.

References

Ahmad A, Senapati S, Khan MI, Kumar R, Ramani R, Sastry M (2003) Intracellular synthesis of gold nanoparticles by a novel alkalotolerant actinomycete. *Rhodococcus* species. Nanotechnology 14:824

Anshup A, Venkataraman JS, Subramaniam C, Kumar RR, Priya S, Kumar TRS, Omkumar RV, John A, Pradeep T (2005) Growth of gold nanoparticles in human cells. Langmuir 21:11562–11567

Beveridge TJ, Hughes MN, Lee H, Leung KT, Poole RK, Savaidis I, Silver S, Trevor JT (1997) Metal-microbe interactions: contemporary approaches. Adv Microb Physiol 38:177–243

Biesso A, Qian W, El-Sayed MA (2008) Gold nanoparticle plasmonic field effect on the primary step of the other photosynthetic system in nature, bacteriorhodopsin. J Am Chem Soc 130:3258–3259

Brayner R, Barberousse H, Hemadi M, Djediat C, Yéprémian C, Coradin T, Livage J, Fiévet F, Couté A (2007) Cyanobacteria as bioreactors for the synthesis of Au, Ag, Pd and Pt nanoparticles via an enzyme-mediated route. J Nanosci Nanotechnol 7:2696–2708

Dahl J, Maddux BL, Hutchison JE (2007) Toward Greener Nanosynthesis. Chem Rev 107:2228–2269

Dahoumane SA, Djediat C, Yéprémian C, Couté A, Fiévet F, Coradin T, Brayner R (2012) Recycling and adaptation of *Klebsormidium flaccidum* microalgae for the sustained production of gold nanoparticles. Biotechnol Bioeng 109: 284–288

Das SK, Marsili E (2010) A green chemical approach for the synthesis of gold nanoparticles: characterization and mechanistic aspect Environ Sci Biotechnol. doi:10.1007/s11157-010-9188-5

Das SK, Das AR, Guha AK (2009) Gold nanoparticles: microbial synthesis and application in water hygiene management. Langmuir 25:8192–8199

De Corte S, Hennebel T, Verschuere S, Cuvelier C, Verstratet W, Boon N (2011) Gold nanoparticle formation using *Shewanella oneidensis*: a fast biosorption and slow reduction process. J Chem Technol 86:547–553

Eustis S, El-Sayed MA (2006) Why gold nanoparticles are more precious than pretty gold: noble metal surface plasmon resonance and its enhancement of the radiative and nonradiative properties of nanocrystals of different shapes. Chem Rev 35:209–217

Ghirardi ML, Posewitz MC, Maness PC, Dubini A, Yu J, Seibert M (2007) Hydrogenases and hydrogen photoproduction in oxygenic photosynthetic organisms. Ann Rev Plant Biol 58:71–91

Grzelczak G, Pérez-Juste J, Mulvaney P, Liz-Marzán LM (2008) Shape control in gold nanoparticle synthesis. Chem Soc Rev 37:1783–1791

He S, Guo Z, Zhang Y, Zhang S, Wang J, Gu N (2007) Biosynthesis of gold nanoparticles using the bacteria *Rhodopseudomonas capsulate*. Mater Lett 61:3984–3987

Hennebel T, Verhagen P, Simoen H, De Gusseme B, Vlaeminck SE, Boon N, Verstraete W (2009) Remediation of trichloroethylene by bio-precipitated and encapsulated palladium nanoparticles in a fixed bed reactor. Chemosphere 76:1221–1225

Hudson RJM, Morel FMM (1993) Trace metal transport by marine organisms: implications of metal coordination kinetics. Deep Sea Res 40:129–150

Jaouen V, Brayner R, Lantiat D, Steunou N, Coradin T (2010) In situ growth of gold colloids within alginate films. Nanotechnology 21:185605

Klaus-Joerger T, Joerger J, Olsson E, Granqvist CG (2001) Bacteria as workers in the living factory: metal-accumulating bacteria and their potential for materials science. Trends Biotechnol 19:15–20

Korbekandi H, Iravani S, Abbasi S (2009) Production of nanoparticles using organisms. Crit Rev Biotechnol 29:279–306

Kumar SA, Abyaneh MK, Gosavi SW, Kulkarni SK, Pasricha R, Ahmad A, Khan MI (2007) Nitrate reductase-mediated synthesis of silver nanoparticles from $AgNO_3$. Biotechnol Lett 29:439–445

Lang NJ, Fay P (1971) The heterocysts of blue-green algae. II. Details of ultrastructure. Proc R Soc Lond B 178:193–203

Lengke M, Southam G (2006) Bioaccumulation of gold by sulfate-reducing bacteria cultured in the presence of gold(I)-thiosulfate complex. Geochim Cosmochim 70:3646–3661

Lengke MF, Ravel B, Fleet ME, Wanger G, Gordon RA, Southam G (2006) Mechanisms of gold bioaccumulation by filamentous cyanobacteria from gold(III)–chloride complex. Environ Sci Technol 40:6304–6309

Mandal D, Bolander ME, Mukhopadhyay D, Sarkar G, Mukherjee P (2006) The use of microorganisms for the formation of metal nanoparticles and their application. Appl Microbiol Biotechnol 69:485–492

Mann S (2008) Life as a nanoscale phenomenon. Angew Chem Int Ed 47:5306–5320

Moulton MC, Braydich-Stolle LK, Nadagouda MN, Kunzelman S, Hussain SM, Varma RS (2010) Synthesis, characterization and biocompatibility of "green" synthesized silver nanoparticles using tea polyphenols. Nanoscale 2:763–770

Narayanan KB, Sakthivel N (2010) Biological synthesis of metal nanoparticles by microbes. Adv Colloid Interface Sci 156:1–13

Reddy KM, Feris K, Bell J, Wingett DG, Hanley C, Punnoose A (2007) Selective toxicity of zinc oxide nanoparticles to prokaryotic and eukaryotic systems. Appl Phys Lett 90(213902–1):213902–213903

Ritchie RJ (2008) Fitting light saturation curves measured using modulated fluorometry. Photosynth Res 96:201–215

Sheng GP, Yu HQ, B Z, Yue ZB (2005) Production of extracellular polymeric substances from *Rhodopseudomonas acidophila* in the presence of toxic substances. Appl Microbiol Biotechnol 69:216–222

Sicard C, Brayner R, Margueritat J, Hémadi M, Couté A, Yéprémian C, Djediat C, Aubard J, Fiévet F, Livage J, Coradin T (2010) Nano-gold biosynthesis by silica-encapsulated micro-algae: a "living" bio-hybrid material. J Mater Chem 20:9342–9347

Sudesh K, Abe H, Doi Y (2000) Synthesis, structure and properties of polyhydroxyalkanoates: biological polyesters. Prog Polym Sci 25:1503–1555

Thomson N, Summers D, Sivaniah E (2010) Synthesis, properties and uses of bacterial storage lipid granules as naturally occurring nanoparticles. Soft Matter 6:4045–4057

Vijayakumar PS, Prasad BLV (2009) Intracellular biogenic silver nanoparticles for the generation of carbon supported antiviral and sustained bactericidal agents. Langmuir 25: 11741–11747

Vijayaraghavan K, Mahadevan A, Sathishkumar M, Pavagadhi S, Balasubramanian R (2011) Biosynthesis of Au(0) from Au(III) via biosorption and bioreduction using brown marine alga *Turbinaria conoïdes*. Chem Eng J 167: 223–227

Virkutyte J, Varma RS (2011) Green synthesis of metal nanoparticles: biodegradable polymers and enzymes in stabilization and surface functionalization. Chem Sci 2:837–846

Wong SL, Nakamoto L, Wainwright JF (1994) Identification of toxic metals in affected algal cells in assays of wastewaters. J Appl Phycol 6:405–414

Wu LQ, Payne GF (2004) Biofabrication: using biological materials and biocatalysts to construct nanostructured assemblies. Trends Biotechnol 22:593–599